Proceedings World Geothermal Congress 2023
Beijing, China, October 17 – 21, 2023

Development of Chloride-based Inflow Detection Measurement in Fractured Enhanced Geothermal Systems (EGS) Wells

Sarah Sausan[1], Luthfan Hafizha Judawisastra[1], Jiann-cherng Su[2], Roland N. Horne[1]

[1]Dept. of Energy Science and Engineering, Stanford University

[2]Sandia National Laboratories

sausan@stanford.edu, luthfan@stanford.edu, horne@stanford.edu, jsu@sandia.gov

Keywords: chloride concentration, feed zone, fracture inflows, single phase, EGS, Utah FORGE

ABSTRACT

The ongoing development of a chloride-based inflow measurement tool to detect inflow in fractured Enhanced Geothermal Systems (EGS) wells has shown promising results that are presented in this paper. The tool is designed to detect and quantify inflows from individual fractures in EGS wells to characterize the events of stimulations, with an application at Utah FORGE (Frontier Observatory for Research in Geothermal Energy), and ultimately at other EGS sites. A successful development of the chloride tool will greatly reduce uncertainty in EGS well development and help in making EGS more commercially attractive.

A new version of the chloride tool is being built and will be tested against high-pressure and high-temperature conditions, specifically at 207 MPa and 225°C. Meanwhile, dye-tracer experiments in a model wellbore confirm the flow behaviors observed in the numerical simulation results. Dynamic measurement was performed with motion of the tool running in and pulling out of the well and with the tool positioned at the wellbore center and at the opposite wall from the feed zone inlet. Comparable cases were also simulated numerically for comparison. Overall, the simulation results of the state when the tool is in place agreed with the experimental measurement, especially on observing the peak chloride concentration at the feed zone height. Differences were found in the measured concentration, which suggests that the calibration equation be reexamined, especially considering the overestimation that was registered when the tool was placed at the center. Simulations also showed that measurement zones apparent in the high inlet flowrate cases are less so in the low inlet flowrate cases, albeit the inlet front peak can still be detected. Furthermore, simulation of various tool position scenarios indicated inlet front peak chloride concentrations only being seen within the feed zone ”jet”. Overall, the recent findings support the inclusion of a centralizer for the wireline tool design to increase the consistency and precision of the chloride concentration calculation.

1. INTRODUCTION

An Enhanced Geothermal System (EGS) requires artificial fractures to be created in low-permeability rocks via stimulation (Huenges, 2016). After such fractures are created, it is essential to monitor their effectiveness over the life of the well, and additional stimulations might be needed to maintain the productivity level. The pressure-temperature spinner (PTS) tool is commonly used to measure the inflow rate from the feed zones. However, the PTS tool is often inconsistent in low fluid velocity, low enthalpy, and big-diameter wells (Acuña and Arcedera, 2005).

This research modified and expanded upon a previous study by Gao et al. (2017) to apply to EGS wells, particularly for the Utah FORGE conditions and configurations in which field tests will be conducted. In the previous study, feed zone enthalpy was measured by proxy of voltage measurement taken using the ion-selective electrode. Chloride was chosen as the species to be measured because chloride always remains in the liquid phase. A change in chloride concentration reflects a change in steam fraction. In this study, the feed zone inflow rate was the target rather than enthalpy as the approach would be applied for single-phase flow with the primary objective of locating and quantifying feed zones in enhanced geothermal wells. Four methods were used to determine optimal tool design and measuring techniques: analytical derivations, laboratory experiments, numerical flow simulations, and field tests.

The analytical approach and field test preliminary data analysis has been detailed in Sausan et al. (2022), while preliminary data analysis pointed out well 58-32 as the most suitable candidate for the field test at Utah FORGE. Laboratory experiments and numerical simulation progress were outlined in Judawisastra et al. (2022), highlighting the calibration of the chloride tool, the measurement of downhole flow and single feed zone injection, and the results of dye-tracer tests. Additionally, the numerical simulation cases ranging showed an agreement of simulation results with the laboratory experiments. This paper outlines the current update on the laboratory experiments and numerical flow simulation, as well as the assembly of the new version of the tool prototype by Sandia National Laboratory.

2, TOOL DEVELOPMENT AND ASSEMBLY

The early prototype of the chloride measurement device was developed at Sandia National Laboratory (Cieslewski et al. 2016; Corbin et al. 2017). The device was designed as a wireline tool that infers chloride concentration via voltage measurement using an ion-selective electrode (Figure 1). Using an empirical relationship, the measured voltage is converted into chloride concentration, which can then be used to estimate the feed zone flow rate via a series of mass balance equations detailed by Sausan et al. (2022).

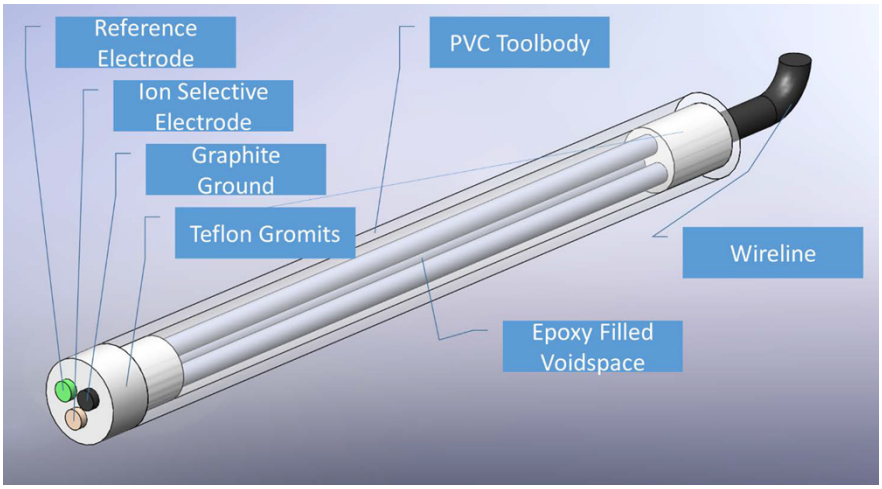

Figure 1: Chloride concentration measurement tool diagram (Gao et al., 2017).

An updated version of the chloride tool is being developed to help with improving voltage-chloride calibration and to test its ruggedness against downhole pressure and temperature conditions expected at Utah FORGE. Like the earlier prototype, the ion-selective probe in the new tool version also generates a voltage proportional to the chloride concentration in the fluid. Meanwhile, the reference electrode provides the reference potential for the pair.

The chloride tool contains sensors fabricated from powdered feedstocks, which are pressed in die presses. A close-up view of the reference electrode is shown in Figure 2. The reference electrode consists of a transducer, baffle, and membrane. The membrane is a mixture of potassium chloride pressed with bonding agents. The material is pressed in a pellet press and heated to bond to the baffle. The baffle is a pressed mixture of silver chloride and potassium chloride powder. The transducer consists of silver-coated graphite spheres pressed onto the baffle. A conductor rod is bonded to the transducer and connects outside the sealed portion of the autoclave to extract the reference signal.

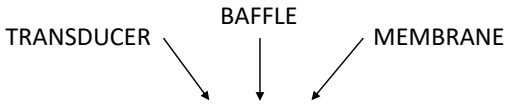

Figure 2: Reference electrode features.

The ion-selective electrode is shown in Figure 3. It is constructed in a similar fashion to the reference electrode. However, the sensor pellet is pressed from a combination of silver sulfide and silver chloride powders. The sensor is sealed in the autoclave via a PTFE liner and compression-style tube fitting.

Figure 3: Ion-selective electrode configured for autoclave testing.

Test conditions for the autoclave are listed in Table 1. The pressure and temperature are selected to replicate the anticipated conditions for the deployed tool. The autoclave (Figure 4) allows testing of the sensors in a simulated high-pressure, high-temperature environment before the fabrication of the deployable tool. The sensor's mechanical integrity and high-temperature calibration will be characterized during the autoclave tests. Chloride concentration will be adjusted by injecting a brine solution into the autoclave under pressurized conditions.

Table 1. Target conditions for autoclave testing

Pressure	20.7 MPa (3000 psi)
Temperature	225°C (437°F)
Chloride concentration	XX%-YY%

Autoclave

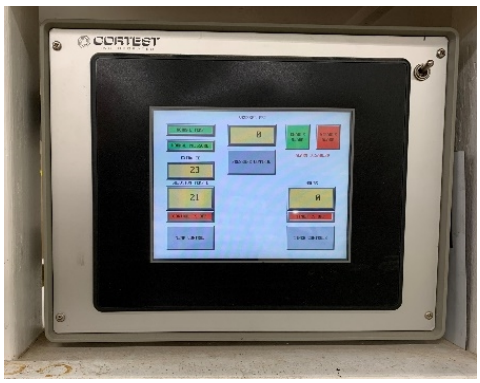

Autoclave controller

Figure 4: Sandia Autoclave and Controller.

3 LABORATORY EXPERIMENTS

Laboratory experiments were conducted in parallel with numerical simulations to evaluate the tool's feasibility under various wellbore configuration scenarios and to design the appropriate operational procedure for the field test.

3.1. Preceding Laboratory Experiments Results

A summary of the preceding experiment results, as outlined in Judawisastra et al. (2022), is given as follows:

a. Chloride tool calibration

The calibration experiments resulted in the empirical relationship between voltage and chloride concentration to be:

$$-\log(M) = 98.58V + 0.2998 \quad (1)$$

where M and V are chloride concentration in mol/L and voltage in volts, respectively.

This relationship is in line with the previous research by Gao et al. (2017), in which higher chloride concentration corresponded with smaller voltage measurements; however, the rate is over twice as steep. It was postulated that the discrepancy was due to device and electrode aging over the five years since the last calibration was performed, thus warranting a new version of the tool to be fabricated.

b. Static measurement

To simulate field conditions, experiments using the chloride tool were designed with varying wellbore and feed zone configurations using the artificial well system at Stanford Geothermal Laboratory. The first experiments were conducted by flowing the main wellbore without injection ports. Varying chloride concentrations flowed through the wellbore, and measurement was recorded by placing the chloride tool in the tank, then inside the wellbore. The result was satisfactory up to 0.4 mol/L, as the chloride concentration calculated using the voltage-chloride relationship (Equation 1) is comparable to the known chloride concentration. However, beyond that, the results are less in agreement. Adding more data points at higher chloride concentrations would help confirm the empirical relationship's validity.

The next series of experiments involved activating one of the injection ports to simulate inflow from a feed zone. The main reservoir tank was filled with fresh water, while a secondary 20 L tank supplied the feed zone with chloride solution at

three different concentrations: 0.1 mol/L, 0.5 mol/L, and 1 mol/L. The chloride tool was suspended from above, and the electrode end was placed close to the feed zone at the center of the wellbore. The result shows that generally, the voltage measurement stabilized 2.5 minutes after injection was started, which was a considerable amount of time for a wireline operation. It was also observed that the final measurement still underestimated the actual chloride concentration, which worsened with smaller values of concentration. The underestimation seemed to be due to nonuniform mixing or suboptimal placement, i.e., the tool was too far from the feed zone mouth.

c. Dye tracer test

The dye tracer test was performed to understand better the flow dynamics and fluid mixing behavior at the well. Instead of injecting chloride solution as in the previous experiments, blue-dyed fresh water was injected at a rate of 100 ml/s. The essential flow features observed from the dye-tracer test are shown in Figure 5. The inflow fluid initially flowed across the wellbore, hitting the opposite side of the wall, then moving upwards following the direction of wellbore circulation. Then, a blind spot appeared, showing a region at which measurement would underestimate the injected chloride concentration. Furthermore, the presence of turbulence was indicated by erratic up-and-down movement and alternating paths from curved to straight. At 55 seconds, the main wellbore was entirely blue, with complete mixing due to the fluid recirculation.

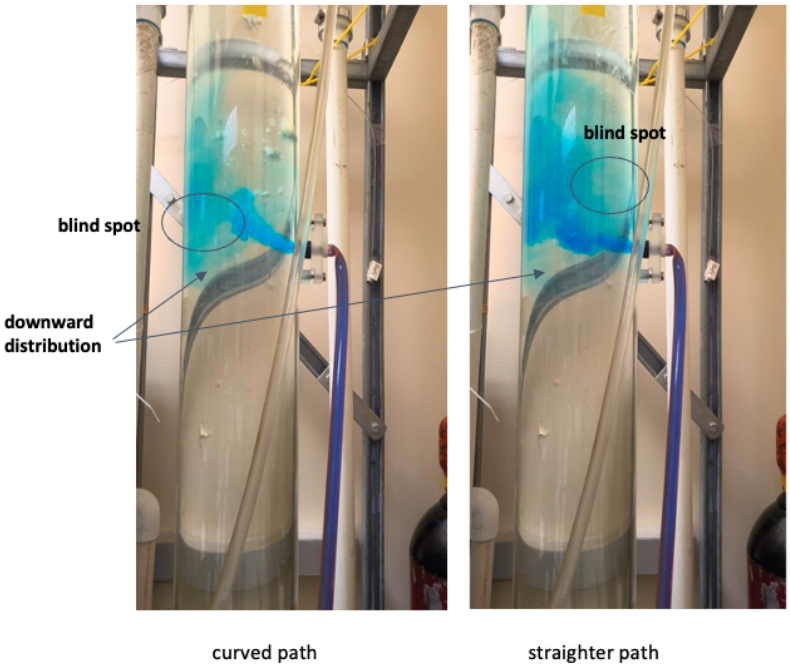

Figure 5: Important features observed from the dye tracer test

3.2. Updated Laboratory Experiment Results

3.2.1 Static Measurement

Another static measurement was performed as a follow-up, with different tool placements: at the center of the wellbore (Position 1) and right in front of the feed zone (Position 2) using the same 0.1 mol/L of chloride solution injection from the feed zone. The result is shown in Figure 6, indicating a significant pattern of measurement observed with Position 2 yielding a much more accurate measurement. Considering that Position 2 could be challenging to achieve in real-life deployment, we would like to explore the range of distance from the feed zone mouth at which the measurement is still acceptably accurate.

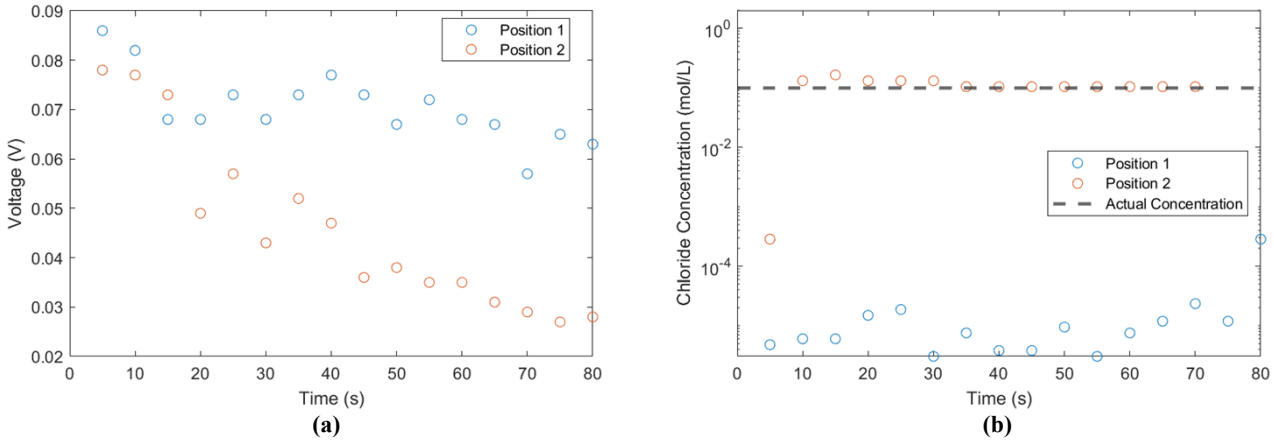

Figure 6: Different tool placement experiments: (a) voltage measurement result, and (b) comparison between calculated and actual chloride concentration values.

3.2.3 Dye-tracer Test

In addition to the side view observation of the dye-tracer test, a cross-sectional perspective was also achieved by lowering an underwater camera into the flow. Figure 7 shows the cross-sectional view of the blue injection fluid mixed into the wellbore with a 0.5-second increment. The left column of Figure 7 shows the actual footage, the middle column shows brightness- and contrast-adjusted footage, and the right column shows the blue dye filter distribution in black. The small red rectangle represents the injection port, while the circle represents the circumference of the well at the injection port depth. The white rings appearing in the left and middle columns are air bubbles stuck on the camera lens, affecting the clarity of the view. Still, the original footage shows the mixing of the blue dye into the wellbore region. Moreover, Figure 7c taken at 1 second shows the injection fluid was reaching the opposite side of the injection port and swirling to the sides, confirming the observation of the side view. This was followed by the circling of dye around the perimeter becoming more extensive over time.

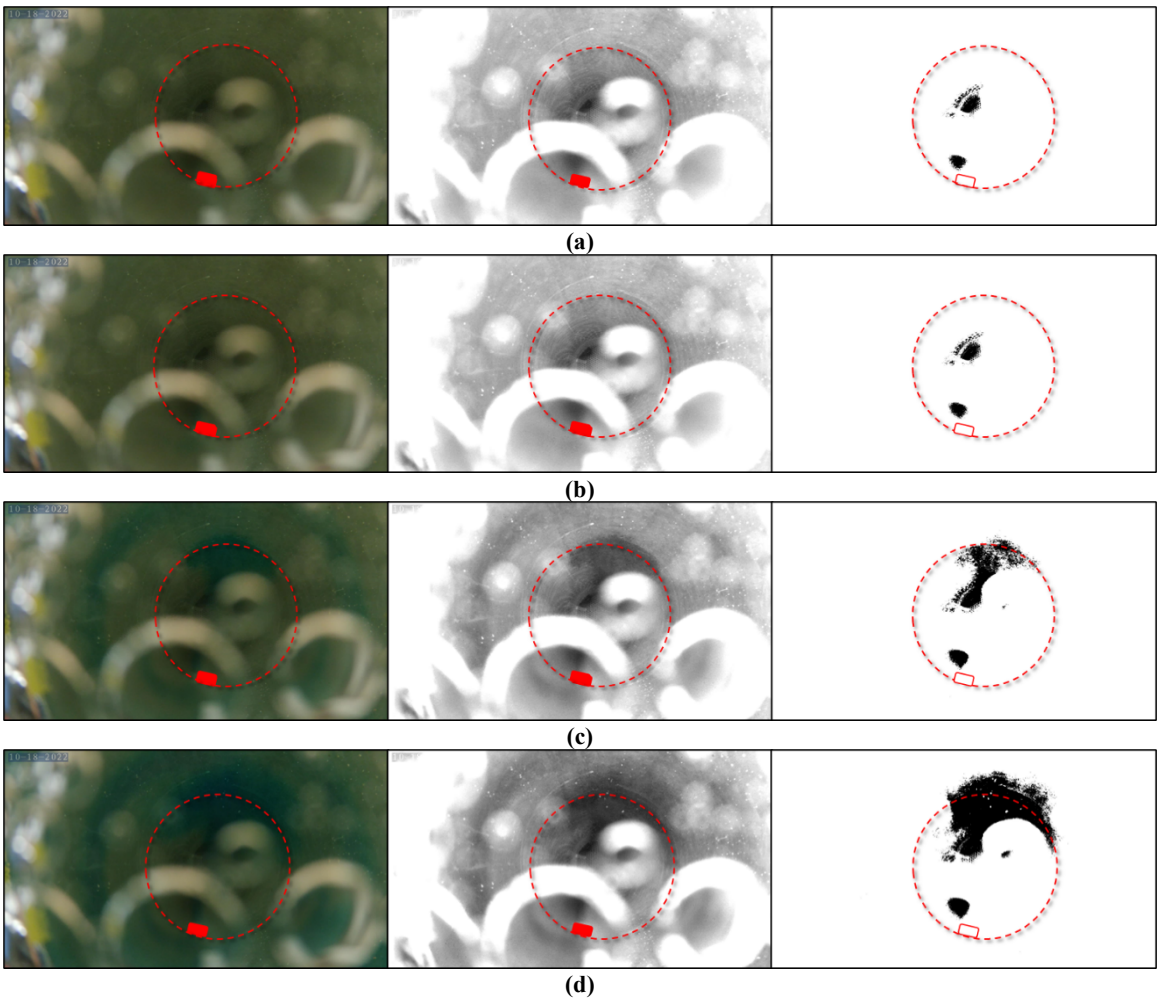

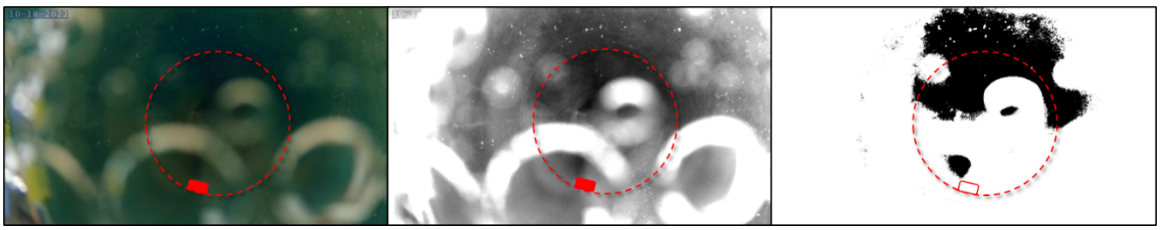

(e)

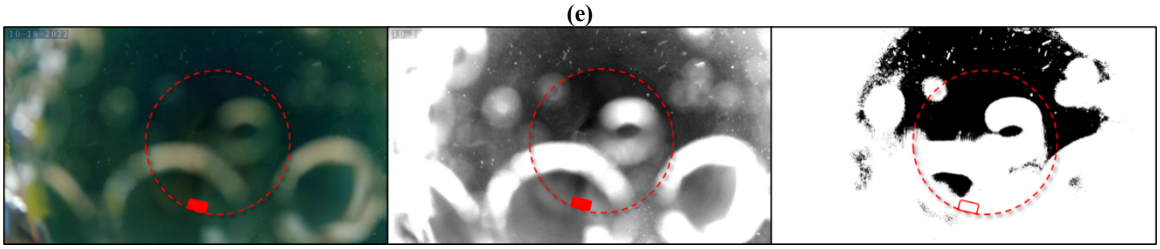

(f)

Figure 7: Dye tracer test cross sectional view over time (a) 0 second, (b) 0.5 seconds, (c) 1 seconds, (d) 1.5 seconds, (e) 2 seconds, (f) 2.5 seconds.

Dye tracer tests were conducted under different flow rates of 20, 50, and 70 ml/s with similar downhole flow conditions to further understand the flow behavior response. After the flow was relatively steady, a blind spot directly above the feed zone port was also replicated on the 70 ml/s test (Figure 8c), indicated by the red circle. However, the blind spot did not appear in the 20 and 50 ml/s cases. During the 20 ml/s test (Figure 8a), injection fluid tends to stay on the injection port side wall and have less mixing with the downhole flow, while during the 50 ml/s test (Figure 8b), the flow goes upward around a third of the well diameter leaving an area without mixing at the other end of the well diameter. The result of this experiment suggests that a higher flow rate produces a blind spot directly above the feed zone inlet, while a low flow rate produces a blind spot across from the injection port. The findings are in line with the blind spots appearance in numerical simulations conducted at low to high feed zone inflow rates, as shown in Judawisastra et al. (2022).

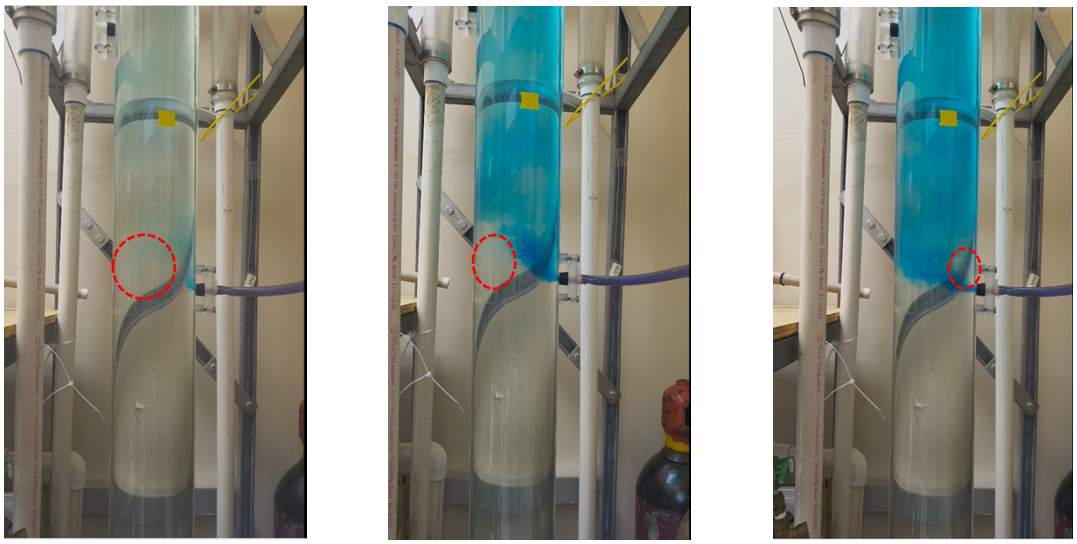

(a) **(b)** **(c)**

Figure 8: Dye injection tracer test (a) 20 ml/s, (b) 50 ml/s, (c) 70 ml/s

3.2.3 Dynamic Measurement

The dynamic tests in the laboratory were conducted to mimic the field measurement, where chloride measurement will be taken along the wellbore using a downhole logging tool attached to a wireline. The laboratory tests were conducted by running the tool into the artificial wellbore system, starting from the top to nearly the bottom of the well (run-in hole or RIH) and then pulling the tool back up (pull-out of hole or POOH). The tool was lowered and pulled at 150 cm/minute. Due to the artificial well system limitations, the measurements were not conducted for the whole section below the feed zone. Two measurements were performed under different tool positions. The first measurement was conducted with the tool close to the opposite wall of the injection port (Figure 9a). The second measurement was run with the tool placed at the center of the wellbore, aided by a centralizer (Figure 9b). The fluid concentration from the injection port was 0.05 mol/L with a flow rate of around 100 ml/s, while the main wellbore flow was zero chloride concentration with the same 2.09 kg/s mass rate.

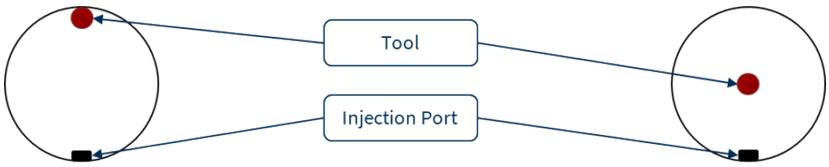

(a) **(b)**

Figure 9: tool position during the dynamic measurement as seen from the XY section: (a) across the injection port, and (b) centralized.

The results of both dynamic measurements are presented in Figure 10. The measured voltage from the tool was converted into chloride concentration using Equation 1. Both measurements successfully captured the drop in voltage around the injection port, indicating a spike of chloride concentration around that depth. The calculated chloride concentration also showed promising results, being close to 0 mol/L below and increasing around and above the feed zone. However, a portion of the calculated chloride concentration around and above the feed zones shows values higher than the possible value of 0.05 mol/L, which is the chloride concentration being injected.

Moreover, it was also observed that the centralized position generally measures higher concentration at similar depths compared to the first position, which indicated that less mixing happened further away from the feed zone. Lastly, it was also noticed that there was a delay in response of the tool shown by the consistently different depth of peak measurement between the RIH and POOH. The RIH measurement suggested a peak below the feed zone, while the POOH shows it above the feed zone. These findings indicate that the dynamic measurement protocols need to be incorporated, especially regarding the time response and chloride concentration accuracy.

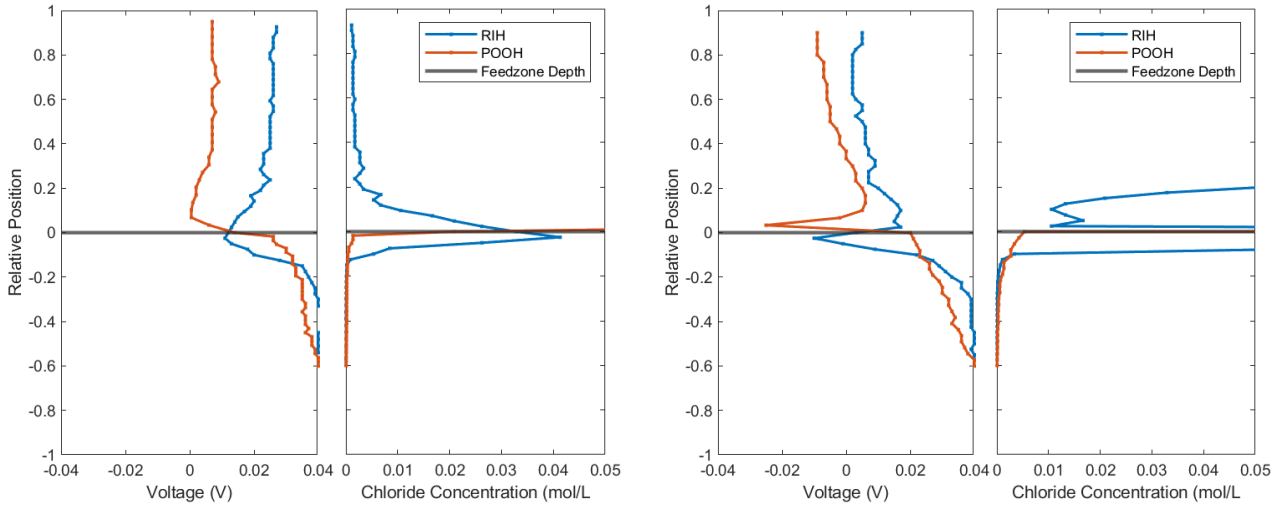

(a) **(b)**

Figure 10: Dynamic measurement result (a) at the opposite wall from the feed zone inlet, and (b) at the center of the wellbore.

4. NUMERICAL FLOW SIMULATION

The numerical flow simulation was conducted in support of the laboratory experiments as well as to expand the investigation into conditions that were difficult to create in the laboratory. For instance, the downhole temperature at the Utah FORGE site may reach as high as 230 °C with different feed zone configurations than those readily available in the artificial well system. From the downhole camera survey analysis at the EGS Collab outlined in Fu and Morris (2020), various feed zone designs should be considered, ranging from a singular jetting point to a fracture plane. A wellbore model with one feed zone was used for the first set of simulations. The numerical simulation was conducted to replicate the laboratory scale, designed to be as close as possible to the laboratory experiments so that a comparison can be drawn. It is worth noting however that the laboratory well model is very close in size to the actual well at Utah FORGE.

Simulation cases were designed to capture varying mass flow Δm at varying chloride concentration ΔCl (Equations 2 and 3), i.e., the difference between main wellbore chloride concentration and feed zone chloride concentration. Both variables are proxies of the chloride tool resolution and accuracy, particularly the smallest feed zone chloride signal the tool can be expected to pick up and the farthest from the feed zone where the chloride tool could be placed.

$$\Delta m = m_{main\ wellbore} - m_{feed\ zone\ inflow} \tag{2}$$

$$\Delta Cl = Cl_{feed\ zone\ inflow} - Cl_{main\ wellbore} \tag{3}$$

A summary of preceding simulation results outlined by Judawisastra et al. (2022) is presented and followed by the updated simulation results.

4.1 Preceding Simulation Results

As outlined in Judawisastra et al. (2022), four case groups were examined for Model S1 with a singular jetting point. The cases configuration and a summary of results are as follows:

- The S1-L1 case group was set up with internal flow at up to 6.7 kg/s and a closed wellhead valve. This case represented a condition where the internal wellbore flow is much larger than the inflow, i.e., large Δm. The simulation showed that feed zone inflow could not enter the main wellbore; instead, backflow into the feed zone inlet occurred.
- The S1-L2 case group was set up with a static wellbore, i.e., with no internal flow and a closed wellhead valve. This case group represented a condition where the feed zone inflow is much more significant than the internal wellbore flow, i.e., negative Δm. The simulation result showed that the path lines exhibited excellent mixing behavior at the feed zone mouth, even with a minimal influx at 20 ml/s.
- The S1-L3 case group was set up with internal flow at 2.09 kg/s, closed wellhead valve, and varying feed zone inflow rate between 20 ml/s to 200 ml/s. This case group was similar to the laboratory experiments setup except for the wellhead where it was kept flowing during the experiments. The cases showed that the feed zone inflow could only enter the wellbore starting at a 70 ml/s rate.
- The S1-L4 case group was set up with internal flow at 2.09 kg/s, wellhead valve open, and varying feed zone inflow rate between 5 ml/s to 200 ml/s. This case group is the closest to the laboratory experiments. In these cases, the inflow could enter the wellbore at 20 ml/s rate and showed prominently in the wellbore starting at 50 ml/s rate.

It was found that the laboratory dye-tracer experiments were the most comparable to the 200 ml/s inflow rate cases at both S1-L3 and S1-L4 case groups. Key features observed in the experiments, such as feed zone inflow hitting the opposite of the wall followed by downward dispersion, formation of blind spots, and periodic turbulence, can also be reproduced in cases S1-L3-5. However, the dye tracer experiment was conducted at around 110 ml/s feed zone inflow rate, meaning that the simulation results underestimated the flow behavior.

4.2 Updated Simulation Results

The updated study aimed to overcome the discrepancy between numerical simulations and laboratory experiments while also expanding the approach to now consider the disturbed state, i.e., the state where the flow behavior in the wellbore is affected by the presence of the chloride tool. An updated geometry setup for the numerical simulations is shown in Figure 11. The feed zone radius is now slightly smaller at 0.5 cm and the well radius is larger at 7.5 cm, compared to what was shown in Judawisastra et al. (2022). The modifications better reflect the artificial well system in the laboratory.

Three new case groups were added, as described in Table 2. Case group S1-L5 examined a smaller feed zone radius at 0.7 cm, 0.5 cm, and 0.1 cm, where the S1-L15-0 case with 0.7 cm radius is the control case of the previous geometry setup. The simulation run on an increasingly smaller feed zone radius was conducted to understand the smallest resolution at which the chloride tool could detect a feed zone. Meanwhile, the S1-L6 case group replayed the S1-L4 cases with a new wellbore radius at 7.5 cm, a new feed zone inlet radius at 0.5 cm, and a denser feed zone inflow rate range between 20 ml/s to 200 ml/s. Finally, the S1-L7 case group simulated the disturbed state, which is the state where the chloride tool is placed near the feed zone inlet and thus disturbed the flow inside the wellbore. The schematic for the disturbed state cases is shown in Figure 12.

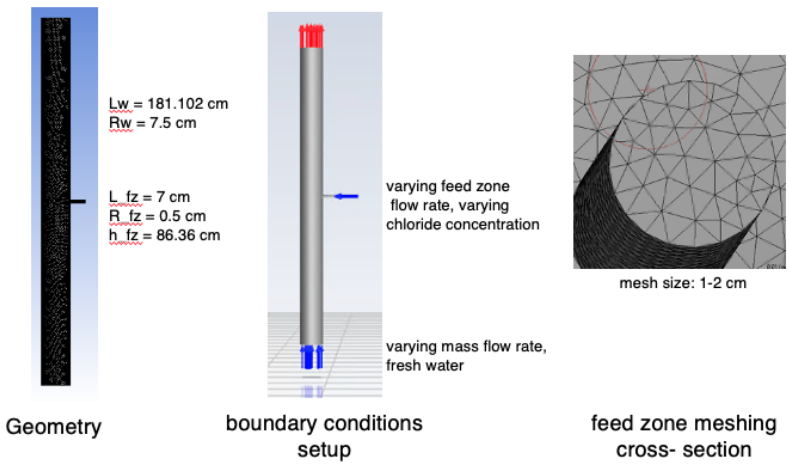

Figure 11: Updated geometry setup and boundary conditions of Model S1 at laboratory scale

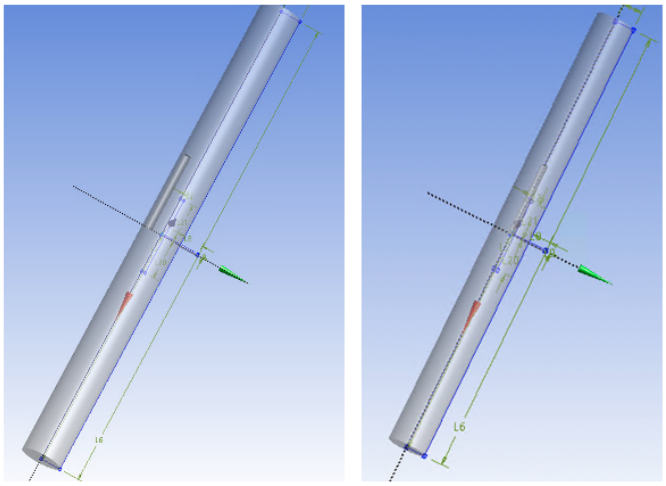

S1-L7-1
Stationary at wall-line-4,
probe end place at inlet mouth

S1-L7-2
Stationary at midline (center), probe
end place at inlet mouth

Figure 12: Schematics and description for the disturbed state case group S1-L7

Table 2: Additional Simulation Case Parameters

Case ID	S1-L5-[0 to 2]	S1-L6-[1 to 9]	S1-L7-[1 to 2]
Scale	Lab scale	Lab scale	Lab scale
Description	Testing different feed zone radius: 0 - R = 0.7 cm 1 - R = 0.5 cm 2 - R = 0.1 cm	Updated geometry setup with different inlet velocity	Disturbed state with stationary chloride tool. Tool position is in the center for case 2a and 2b and 5 cm from the wall at the opposite of the inlet (wall-line-4) for case 1a and 1b.
Wellhead	Open	Open	Open
Main wellbore mass rate	2.09 kg/s	2.09 kg/s	1a & 2a - 2.09 kg/s 1b & 2b – 0 kg/s (no internal flow)
Feed zone flow rate	112.2 ml/s (mimicking lab experiments)	1 - 112.2 ml/s 2 - 125 ml/s 3 - 150 ml/s 4 - 175 ml/s 5 - 200 ml/s 6 - 20 ml/s 7 - 50 ml/s 8 - 75 ml/s 9 - 100 ml/s	112.2 ml/s (mimicking lab experiments)
Δm (kg/s)	1.98	1 – 1.98 2 – 1.96 3 – 1.94 4 – 1.91 5 – 1.89 6 – 2.07 7 – 2.04 8 – 2.01 9 – 1.99	1a & 2a– 1.98 1b & 2b – (-0.112)
NaCl concentration at feed zone	0.05 mol/L	0.05 mol/L	0.05 mol/L
NaCl concentration delta (mol/L)	0.05	0.05	0.05

Upon experimenting with a smaller feed zone inlet radius (Figure 13), slightly decreasing the radius from 0.7 cm (S1-L5-0) to 0.5 cm (S1-L5-1) resulted in a stronger inlet flow that can reach the opposite wall. However, too small of a radius will prevent the inlet fluid from entering the main wellbore as the feed zone flow is weaker than the wellbore's internal flow, as shown in case S1-L5-3. It should be noted that S1 cases are set up with point-source feed zones; other possible feed zone geometries like inclining planes that resemble a fracture intersection may behave differently from the S1-L5 case groups.

Updating the geometry of the well system resulted in a new base case S1-L6-1 which better resembled the laboratory experiments. Features previously only seen in the S1-L4-4 with a 200 ml/s inflow rate, like the prominent blind spot and downward distribution, can now be seen at the 112.2 ml/s inflow rate case. Furthermore, a comparison of lab experiment footage taken from the top of the well with the feed zone fluid volume fraction of the S1-L6-1 case, a horizontal section (Figure 14Figure 14) shows consistent behavior of blind spot formation and inflow fluid reaching the opposite wall followed by circling the perimeter. These similarities mark a step forward in bringing the laboratory experiment and numerical simulation results together.

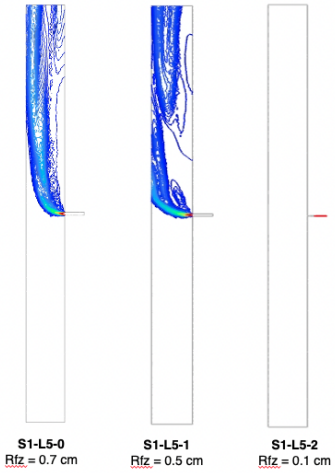

Figure 13: Comparison between S1-L5 cases with different feed zone inlet radius

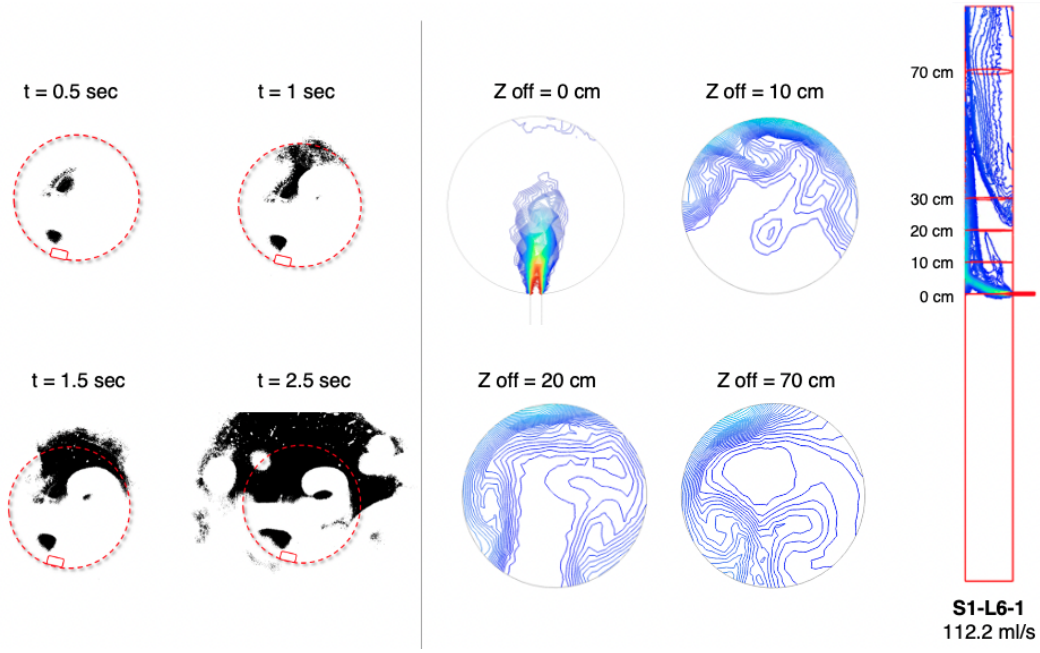

Figure 14: Lab experiment results recorded from the top of the well compared with horizontal sections of the undisturbed state base case S1-L16-1 at different z-offsets. The contours show the volume fraction of the inflow fluid, which is a NaCl solution of 0.05 mol/L concentration.

The result of examining different inflow rates across S1-L6 case groups are summarized in Figure 15. The results are extracted from the wall-line-4 position, which is the position across from the feed zone inlet. The inflow rates are grouped into the high-flowrate group for those more than 112.2 ml/s and the low-flowrate group for those less than 112.2. ml/s. While the high-flowrate group exhibits a clear pattern across the z-direction, i.e., inlet front burst right in front of the feed zone followed by a decrease zone above and topped by rebound zone, the low-flowrate group's pattern is less apparent and more chaotic. One feature in common in both high-flowrate and low-flowrate groups is the inlet front chloride peak, which is promising as we can expect that the chloride tool can consistently locate the feed zone inflow. A similar inlet peak pattern is also observed in the dynamic measurement experiment detailed in Section 3.2.3 and shown in Figure 10a where the tool was also positioned at the wall-line-4 position. A peak in chloride concentration is detected around the feed zone area, marking the position of the feed zone.

As for the magnitude of the chloride concentration, the results all underestimate the incoming 0.05 mol/L concentration to be between 0.01 to 0.017 mol/L or between 20% to 34% of the actual chloride concentration. While it is understood that the dispersed feed zone inflow will inevitably result in diluted chloride concentration when measured at any location of the wellbore except right in front of the inlet, it is expected that the discrepancy will be less pronounced and more consistent in the disturbed state simulation, especially

when the tool is positioned at the center of the wellbore. In actual deployment, there will need to be a compensating correction to the estimated chloride concentration values.

Another comparison can be drawn from the S1-L6 case groups by examining the effect of different tool positions across the wellbore width, as shown in Figure 16. It was found that extracting the chloride concentration results from positions within the feed zone jet, such as from the center of the wellbore (midline position) and the opposite wall (wall-line-4), will produce the inlet front peak pattern that is valuable in locating and quantifying the feed zone inflow. In contrast, extracting results from outside the jet will hide the inlet front peak pattern, making it nearly impossible to pinpoint the feed zone, let alone quantify the flow rate. Thus, the tool design must be able to place the tool firmly within the jets of feed zones along the well, which may be positioned anywhere at the circumference of the wellbore. This feat can be achieved if the tool is kept at the center of the wellbore using a centralizer.

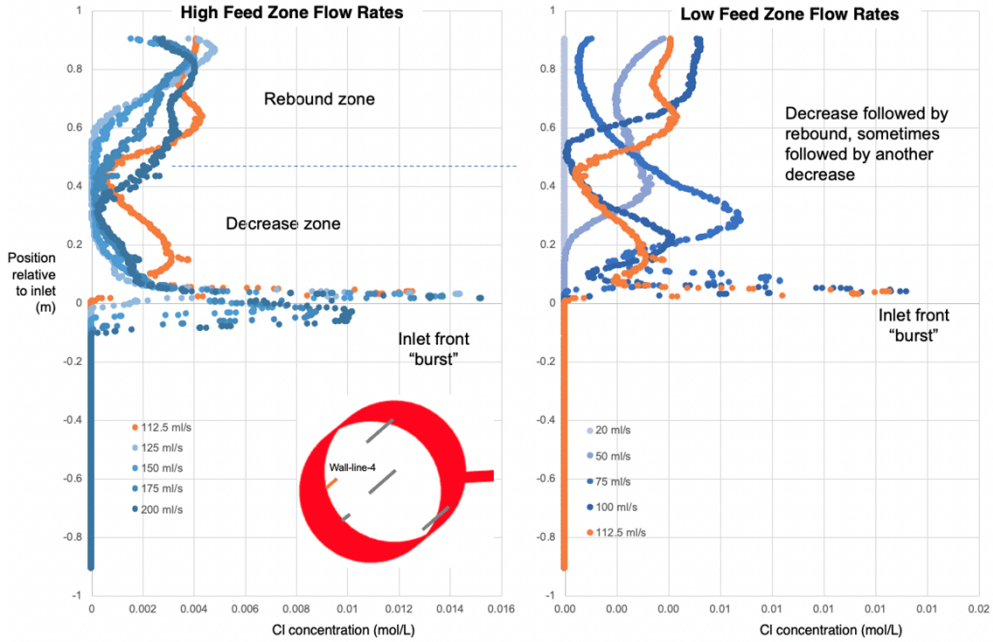

Figure 15: Comparison of the undisturbed state case S1-L6-1 and the Cl concentration change along the wellbore height at different feed zone flow rates. The results are extracted from the wall-line-4 position across the feed zone inlet. The left image shows the base case inlet flow rate (112.2 ml/s) and higher, while the right image shows the base case flow rate and lower.

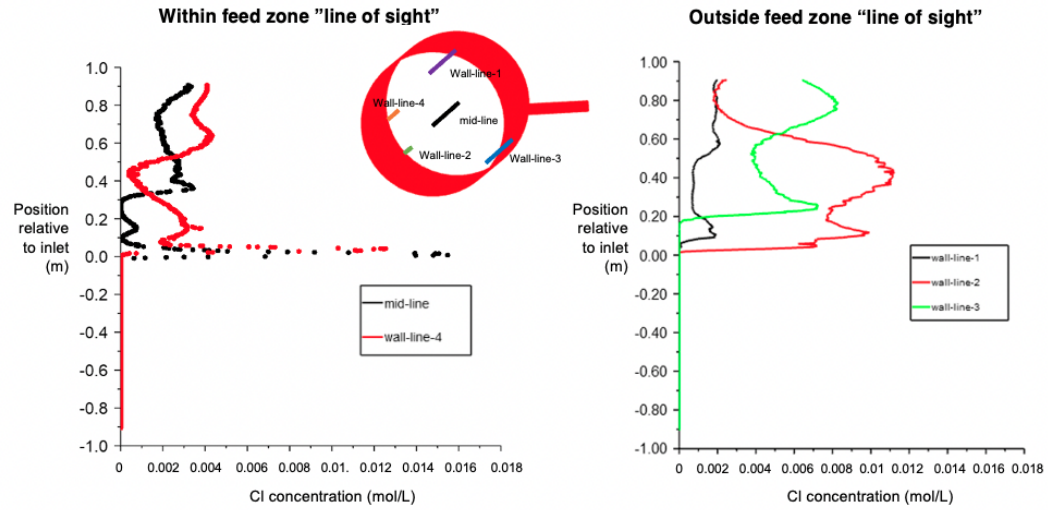

Figure 16: Comparison of the undisturbed state case S1-L6-1 and the Cl concentration change along the wellbore height.

The simulation results of the disturbed state case groups S1-L7 taken from the horizontal section are shown in Figure 17, while the same results in the horizontal section intersected right at the feed zone height are shown in Figure 18. Note that the disturbed state is the most comparable simulation to the dynamic measurement experiment. It can be observed that having the tool placed near the feed zone will pose a significant disturbance to the flow behavior within the wellbore in a positive manner. For instance, putting the tool at the wellbore center (S1-L7-2a) makes the chloride concentration more prominent and closer to the actual inflow concentration at 70-100%. Similarly, placing the tool in the opposite wall (S1-L7-1a) also increases the inflow concentration significantly up to 50%. This finding further supports the use case for a centralizer in the tool design. The S1-L7-1a case can also be compared with the dynamic measurement experiment outlined in Section 3.2.3, although the peak concentration registered during the experiment is much higher than the simulation. Although the inclination is to mark the simulation as underestimating chloride concentration, it

could also be the case that the calibration equation (Equation 1) needs to be revised, as it yields a higher than maximum possible value for when the tool is centered during the dynamic measurement thus overestimating the experiment readings. For the same reason, S1-L7-2a cannot be compared at this point except qualitatively due to the lab experiment registering chloride concentration higher than the maximum possible value.

The results of similar tool placements but with no internal wellbore flow (S1-L7-1b and S1-L7-2b) are also shown. With the lack of upflow, the feed zone fluid is dispersed in all directions instead of uniformly, resulting in a concentration between 30-70%, with inlet flow peak still observed at around 70% concentration. Thus, variation in the internal wellbore flow will affect the quantification of the chloride concentration and, subsequently, the flow rate estimation.

Overall, modeling the disturbed state makes the simulation results more realistic and comparable to the experiments. The disturbed state simulations will be improved by incorporating the wireline assembly design with additional housing units and mixers.

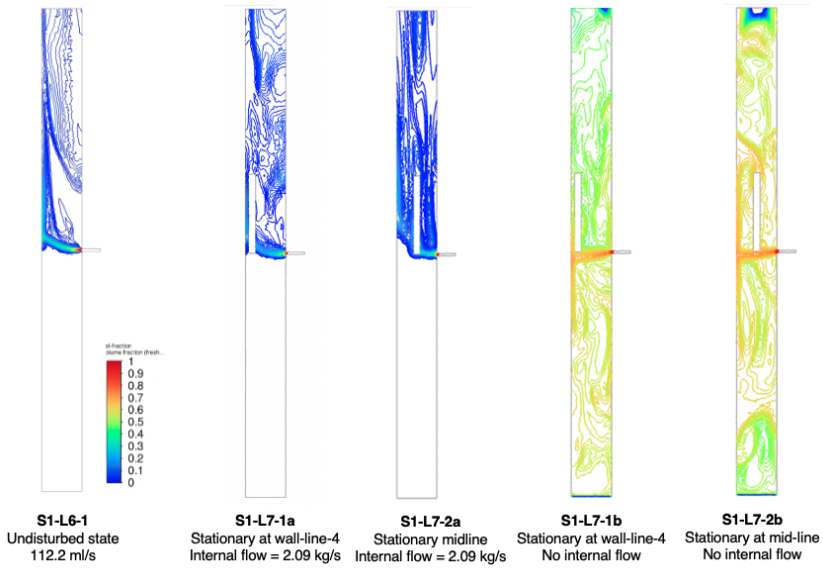

Figure 17: Comparison of the disturbed state case group (S1-L7), XZ section. The contours show the volume fraction of the inflow fluid, which is a NaCl solution of 0.05 mol/L concentration.

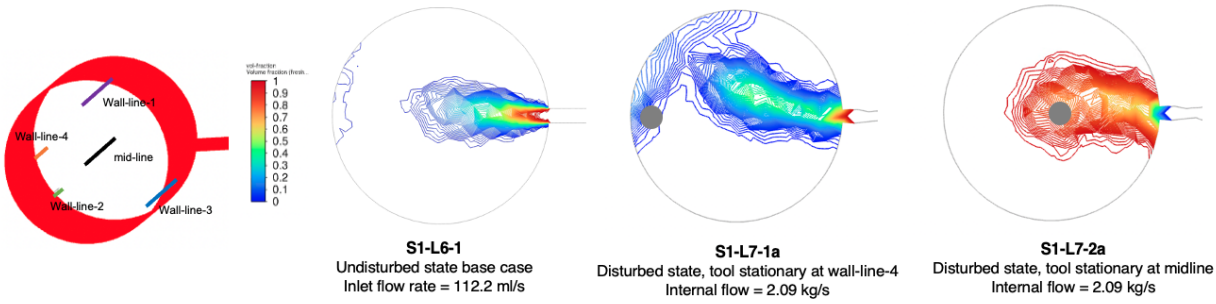

Figure 18: The XY section of the disturbed state cases S1-L7-1a and S1-L7-2a compared with the undisturbed state base case S1-L6-1. Reference to tool position naming is shown in the top left. The contours show the volume fraction of the inflow fluid, which is a NaCl solution of 0.05 mol/L concentration.

5. CONCLUSION

A new version of the chloride tool is being built and will be tested against high-pressure and high-temperature conditions, specifically at 207 MPa and 225°C. Meanwhile, building upon the progress outlined in Sausan et al. (2022) and Judawisastra et al. (2022), a closer look at the dye-tracer experiment in a horizontal cross section confirms the flow behaviors observed in the revised lab-scale simulation. Dynamic measurement was performed with run-in hole and pull-out-of hole motion and with the tool positioned at the wellbore center and at the wall opposite to the feed zone inlet. Comparable cases were also simulated numerically for verification. Overall, the simulation results of the disturbed state (i.e., the state when the tool is in place) agreed with the dynamic measurement in the laboratory, especially on having the peak chloride concentration measured at the feed zone height. Differences were found in the measured concentration, which suggests that the calibration equation should be re-examined, especially considering the overestimation that was registered when the tool was placed at the center.

Simulations also showed that measurement zones apparent in the high inlet flowrate cases are less prominent in the low inlet flowrate cases, although the inlet front peak can still be detected. Furthermore, simulation of various tool position scenarios indicated inlet front peaks only being seen within the feed zone region. Overall, the recent findings support the inclusion of a centralizer for the wireline tool design to increase the consistency and precision of the chloride concentration calculation.

ACKNOWLEDGMENT

This work forms part of the Utah FORGE project under award number 3-2418 as a collaborative project between Stanford University and Sandia National Laboratory, supported by the U.S. Department of Energy.

Sandia National Laboratories is a multimission laboratory managed and operated by National Technology & Engineering Solutions of Sandia, LLC, a wholly owned subsidiary of Honeywell International Inc., for the U.S. Department of Energy's National Nuclear Security Administration under contract DE-NA0003525. This paper describes objective technical results and analysis. Any subjective views or opinions that might be expressed in the paper do not necessarily represent the views of the U.S. Department of Energy or the United States Government.

REFERENCES

Acuña, J. A. and. Arcedera B. A,: Two-Phase Flow Behavior and Spinner Data Analysis In Geothermal Wells, Proceedings 13th Workshop on Geothermal Reservoir Engineering, Stanford University, Stanford, California (2005).

Cieslewski, G., Hess, R. F., Boyle, T. J., Yelton, W. G.: Development of a Wireline Tool Containing an Electrochemical Sensor for Real-time pH and Tracer Concentration Measurement, GRC Transactions, Vol.40, (2016).

Corbin, W. C., Cieslewski G., Hess R. F., Klamm B. E., Goldfarb L., Boyle T. J., and Yelton W.G.: Development of a Downhole Tool for Measuring Enthalpy in Geothermal Reservoirs, 42nd Workshop on Geothermal Reservoir Engineering, Stanford University, Stanford, CA (2017).

Fu, P., Morris, J.: Interpreting EGS Collab Exp. 1 Downhole Camera Survey Results. Geothermal Data Repository. June (2020).

Gao, X., Egan, S., Corbin, W.C., Hess, R.F., Cieslewski, G., Cashion, A.T., and Horne, R.N.: Analytical and Experimental Study of Measuring Enthalpy in Geothermal Reservoirs with a Downhole Tool, GRC Transactions, Vol.41, (2017).

Huenges, E.: 25 - Enhanced geothermal systems: Review and status of research and development, Geothermal Power Generation, Woodhead Publishing, Pages 743-761, (2016).

Judawisastra, L. H., Sausan, S., Horne, R. N.: Analytical, Experimental and Numerical Development Update on Inflow Measurement in Geothermal Wells from Chloride Concentration. Proceedings, 8th Indonesia International Geothermal Convention & Exhibition, (2022).

Sausan, S., Judawisastra, L. H., Horne, R. N.: Development of Downhole Measurement to Detect Inflow in Fractured Enhanced Geothermal Systems (EGS) Wells, Proceedings 47th Workshop on Geothermal Reservoir Engineering, Stanford University, Stanford, California (2022).